Article

Triboelectric tactile sensor for pressure and temperature sensing in high-temperature applications

Yanhua Liu, Jinlong Wang ⓘ, Tao Liu ⓘ, Zhiting Wei, Bin Luo, Mingchao Chi ⓘ, Song Zhang ⓘ, Chenchen Cai ⓘ, Cong Gao, Tong Zhao, Shuangfei Wang & Shuangxi Nie ⓘ ✉

Skin-like sensors capable of detecting multiple stimuli simultaneously have great potential in cutting-edge human-machine interaction. However, realizing multimodal tactile recognition beyond human tactile perception still faces significant challenges. Here, an extreme environments-adaptive multimodal triboelectric sensor was developed, capable of detecting pressure/temperatures beyond the range of human perception. Based on triboelectric nanogenerator technology, an asymmetric structure capable of independently outputting dual signals was designed to improve perception sensitivity. By converting the signals and the stimuli into feature matrices, parallel perception of complex objects (with a recognition rate of 94%) and temperature at high temperatures was achieved. The proposed multimodal triboelectric tactile sensor represents progress in maximum detection range and rapid response, realizing the upper limit of human skin's high-temperature sensing (60 °C) with a working temperature of 200 °C. The proposed self-powered multimodal sensing system offers a wider range of possibilities for human/robot/environment interaction applications.

With the advent of the "artificial intelligence" era, robotics technology provides more convenient and intelligent services for human beings[1–4]. Tactile perception plays a crucial role in the development of intelligent robotic systems, enabling robots to perceive, and analyze external stimuli, or interact friendly with the surrounding environment[5–9]. This perception function is typically achieved through tactile sensors capable of responding to multiple stimuli. The current research on tactile sensors employs various driving mechanisms such as piezoresistive[10], capacitive[11,12], pyroelectric[13], mechanoluminescent[14,15], and piezoelectric[16] to detect physical information, usually working at room temperature. Achieving stable tactile perception in high-temperature harsh environments remains a key challenge beyond the capabilities of existing technologies. Thus, previous studies have primarily focused on the development of tactile sensors in room temperature environments. Multimodal tactile sensors serve as core components in robot perception systems, yet their lack of wide environmental adaptability is the major obstacle restricting the applications of intelligent robots in extreme environments (such as space, deep sea, fire scenes, etc.)[17–19]. Despite the progress in improving high-temperature adaptability by mimicking human tactile receptors (e.g., heterogeneous sensing mechanisms) and advanced material design (e.g., temperature-insensitive sensing materials)[12,20,21] (Supplementary Table 1), limited by the response mechanism of stimulus signals and the design of sensing materials, tactile sensing is still confined to the temperature range of human touch (≤60 °C). Fundamentally, endowing tactile sensors with high-temperature adaptive technology beyond human touch can resolve the challenges of intelligent robot applications in extreme environments, which is urgently needed but not yet solved in practical applications.

Guangxi Key Laboratory of Clean Pulp & Papermaking and Pollution Control, School of Light Industry and Food Engineering, Guangxi University, Nanning 530004, PR China. ✉e-mail: nieshuangxi@gxu.edu.cn

To overcome this challenge, exploring the design strategies for environment-adaptive tactile sensing is necessary. The emerging triboelectric nanogenerator (TENG) technology presents a potential solution to this issue[22–25]. TENG, based on the coupling effects of contact electrification and electrostatic induction, converts tactile stimuli into electrical signals without extra power modules[26–29]. Wang's group found that the transfer of triboelectric charges generated by the contact electrification process exhibits a significant temperature effect, where the increase in temperature enhances the electron emission capability of the layer, resulting in the decrease of the electrical signal of TENG[30]. The temperature dependence of the signal enables the robot to respond to tactile stimuli under high temperatures, which can lay a research foundation for a paradigm of tactile sensing in extreme environments. The works exploring the changes of TENG signals under high-temperature conditions have been reported, such as the clarification of the relationship between the thermionic emission effect and the TENG signal[31], and the design of a self-powered tactile temperature sensor[32], which expanded the application range of temperature sensors. Therefore, based on the temperature dependence and tactile stimulation response of the contact electrification mechanism in TENG, achieving stable tactile perception in extreme environments beyond human tactile perception is feasible. Multimodal sensors are essential for realizing intelligent sensing systems, however, limited by the influence of multiple stimuli, there are still challenges in breaking through multimodal tactile perception under high-temperature environments.

In this work, inspired by Saharan silver ants (*Cataglyphis bombycina*), which are insects capable of maintaining multi-sensory perception in high-temperature environments[33], we develop a triboelectric sensor that enables adaptive tactile sensing under extreme heat, surpassing human tactile limits (Fig. 1a, b). Research indicates that when biological organisms are subjected to mechanical and thermal stimuli, the opening and closing of ion channels generate physiological electric signals, which facilitates environmental perception (Supplementary Fig. 1)[34]. Drawing on this biological principle and based on the contact electrification phenomenon of TENG, a pressure/temperature sensor is designed to sense pressure and thermal stimuli at high temperatures.

Additionally, the triboelectric signals are integrated with machine learning algorithms to achieve object recognition. Thanks to the design of the asymmetric structure and heat-resistant sensing materials, the triboelectric sensor shows fast stress response and recovery times of 70 and 58 ms, respectively. Its maximum operating temperature reaches 200 °C, which far exceeds the human skin's high-temperature sensing limit (60 °C). Furthermore, by integrating the triboelectric sensor on the robotic hand, real-time responses to pressure and temperature under high temperatures are achieved. This research not only solves the long-term challenge of using triboelectricity to achieve accurate pressure and temperature perception at high temperatures, but also promotes the development of efficient intelligent systems in extreme environments.

Results
Design of extreme environment-adaptive triboelectric tactile sensor
Human skin distinguishes mechanical and thermal stimuli through mechanical and temperature receptors, achieving spatiotemporal recognition of the size and location of touch and temperature stimuli[35,36], to ensure safe and effective human-machine interaction in complex environments (Fig. 2a). To simulate natural touch, understanding and utilizing the key factors influencing biological skin sensory characteristics are crucial[20]. Inspired by high-temperature silver ants, as well as skin mechanoreceptors and thermoreceptors along with their sensing mechanisms, taking advantage of charge transfer under external stimuli to generate electrical signals, an extreme environment-adaptive pressure/temperature-responsive triboelectric sensor was designed. The tactile sensor consists of a pressure-sensing triboelectric nanogenerator (P-TENG) and a temperature-sensing triboelectric nanogenerator (T-TENG) (Fig. 2b). Based on the contact electrification principle, the multimodal sensor avoids interference from forces by utilizing the stable contact area of the T-TENG. By exploiting the coupled yet low cross-sensitivity pressure and temperature response mechanisms, it enables the unambiguous discrimination of touch and temperature electrical signals, while showcasing high sensitivity and high-temperature resilience (Fig. 2c),
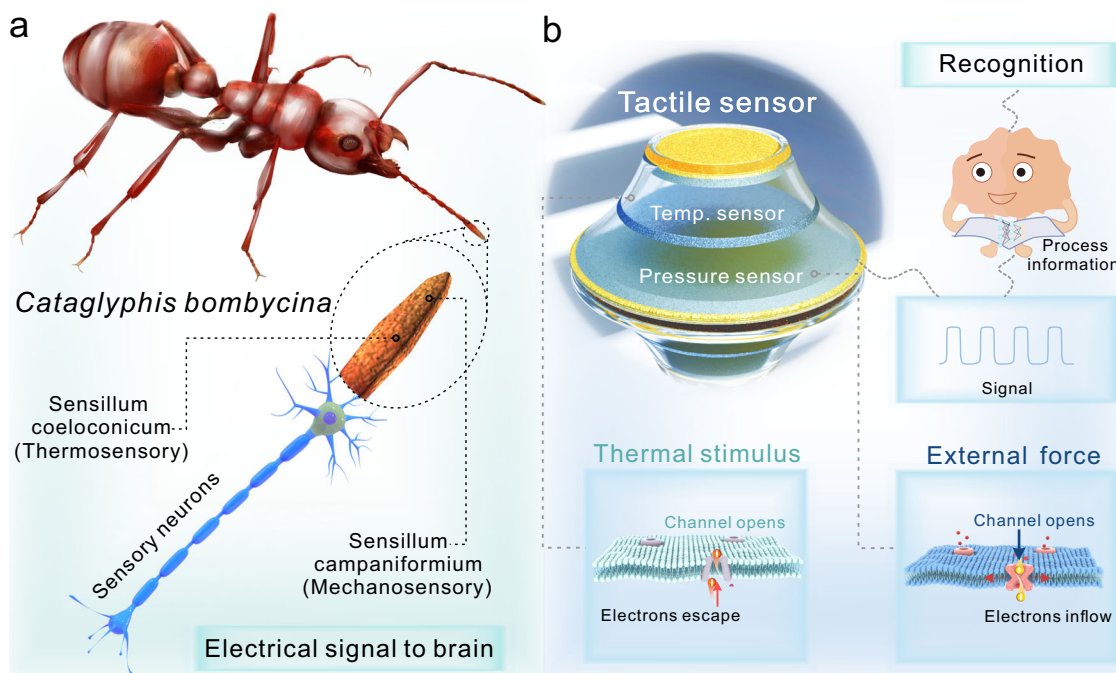

Fig. 1 | Schematic illustration of the bioinspired triboelectric sensor. a Nervous system of the Saharan silver ant for bimodal signals of pressure and temperature under high temperatures. **b** Signals perceived by the triboelectric sensor for machine learning to identify objects.
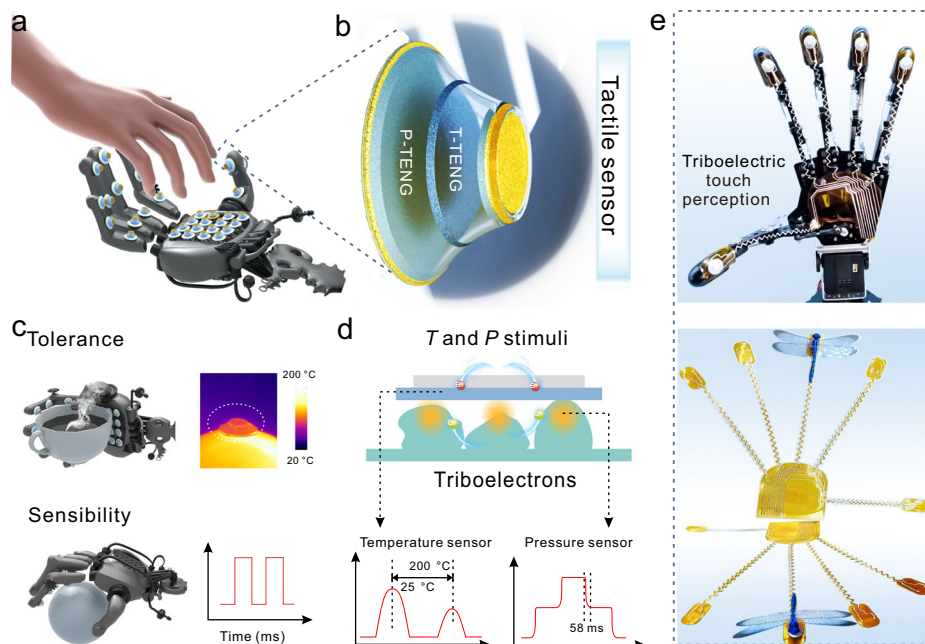
Fig. 2 | Extreme environment-adaptive pressure/temperature-responsive triboelectric sensors beyond human tactile perception. a Schematic illustration of the triboelectric sensor for human-machine interaction. **b** Detailed structure of the sensor, T-TENG, and P-TENG refer to the temperature sensor and pressure sensor. **c** Sensor's high-temperature resistance and sensitivity. **d** Schematic diagram of the principle of sensor response to pressure/temperature, *T* and *P* refer to temperature and pressure. **e** Optical image of the triboelectric sensor integrated on a robotic hand with stretchable electrodes.

providing the possibility for responding to multiple stimuli in extreme environments.

When subjected to pressure and temperature stimuli, the triboelectric materials in the sensor with asymmetric structure contact each other, leading to the charge transfer and further generating corresponding electrical signals (Fig. 2d and Supplementary Fig. 2). To demonstrate the application of triboelectric tactile sensors in object multimodal perception and information feedback, five miniature sensors were assembled on the robotic hand by laser-printed flexible and stretchable electrodes (Fig. 2e), which enables flexible object shape and temperature recognition. The sensor offers broad application prospects for extreme environment-adaptive robots in human-machine interaction, virtual reality, space exploration, etc.

Pressure-responsive behaviors

The preparation process of the triboelectric sensor capable of responding to pressure/temperature in extreme environments is illustrated in Fig. 3a and Supplementary Fig. 3. A structurally asymmetric dual-layer sensor by a two-step encapsulation strategy was designed. To realize adaptive responses in extreme conditions, this work employs flexible, high-temperature-resistant silicone as an outer shell to facilitate rapid responsiveness to pressure stimuli (Fig. 3ai). Additionally, based on the intrinsic high-temperature resistance of cellulose[37], the material was chemically modified and further engineered to develop a spherical-like surface morphology (Supplementary Figs. 4–6), which enhanced the high-temperature triboelectric performance and sensing signals (Supplementary Fig. 7). The cellulose nanofibrils (CNFs-1), with a silver electrode coating on its back, was affixed to the inner surface of the silicone shell at the top (small area side), while fluorinated ethylene propylene (FEP) was adhered and embedded to the middle position inside the shell, the T-TENG was prepared (Fig. 3aii-iv). Finally, a rough-surfaced CNFs-2, also coated with a silver electrode on its back, was affixed to the lower part of the silicone shell, sharing the FEP to construct P-TENG (Fig. 3av), thereby completing the dual-mode sensor (Fig. 3avi). The schematic diagram of P-TENG's amplification is shown in Fig. 3b. When pressure is applied, the FEP makes contact with the protruding spherical structures on the surface of CNFs-2. Due to the coupling effects of triboelectric charging and electrostatic induction, P-TENG can convert mechanical pressure into electrical signals. Additionally, the principle of triboelectric signal generation was further elucidated (Fig. 3c). When the two atoms contact under external force, the electron cloud overlaps, and the electrons of -OH on CNFs-2 film transfer to FEP, thus generating triboelectric charges. The CNFs-2 film accumulated positive charges, generating an output signal, and upon gradual separation, a reverse signal appeared. The variation process of the electric potential on the surface of triboelectric materials was demonstrated through finite element simulation, providing a foundation for detecting pressure-sensitive signals (Supplementary Fig. 8 and Supplementary Movie 1).

The size of the device is constrained by the actual interactive scenarios[38]. Therefore, sensors of different sizes were fabricated, and research revealed that the triboelectric performance increased linearly with the size (Fig. 3d), which was attributed to the increase of contact area, thus transferring more charges during the contact process. The surface roughness structure plays an indispensable role in improving the fast response ability and sensitivity of the pressure sensor[39]. The CNFs-2 film with a microstructure surface facilitates the enhancement and precise analysis of pressure signals (Supplementary Fig. 9 and Supplementary Notes 1, 2). Response time is a prerequisite for measuring the device's response sensitivity, and plays a key role in human-machine interaction in virtual reality environments[40]. When pressure was applied to P-TENG at 2 Hz, the response and recovery times were 70 and 58 ms, respectively (Fig. 3e), and the higher response time is maintained at different frequencies (Supplementary Fig. 10), faster than the human response time to tactile stimuli (139 ms)[6,41]. The triboelectric signals of P-TENG were tested to explore their adaptability to different touch pressures. Figure 3f displays voltage signals of loading and unloading at different pressures from 4.17 to 100 kPa, demonstrating that P-TENG is an ideal candidate for tactile perception. The linear curve of the voltage with pressure change is shown in Fig. 3g. When the pressure is less than 8.36 kPa, the sensitivity of the triboelectric signal is 9.21 kPa^{-1}, and when the pressure is in the range of
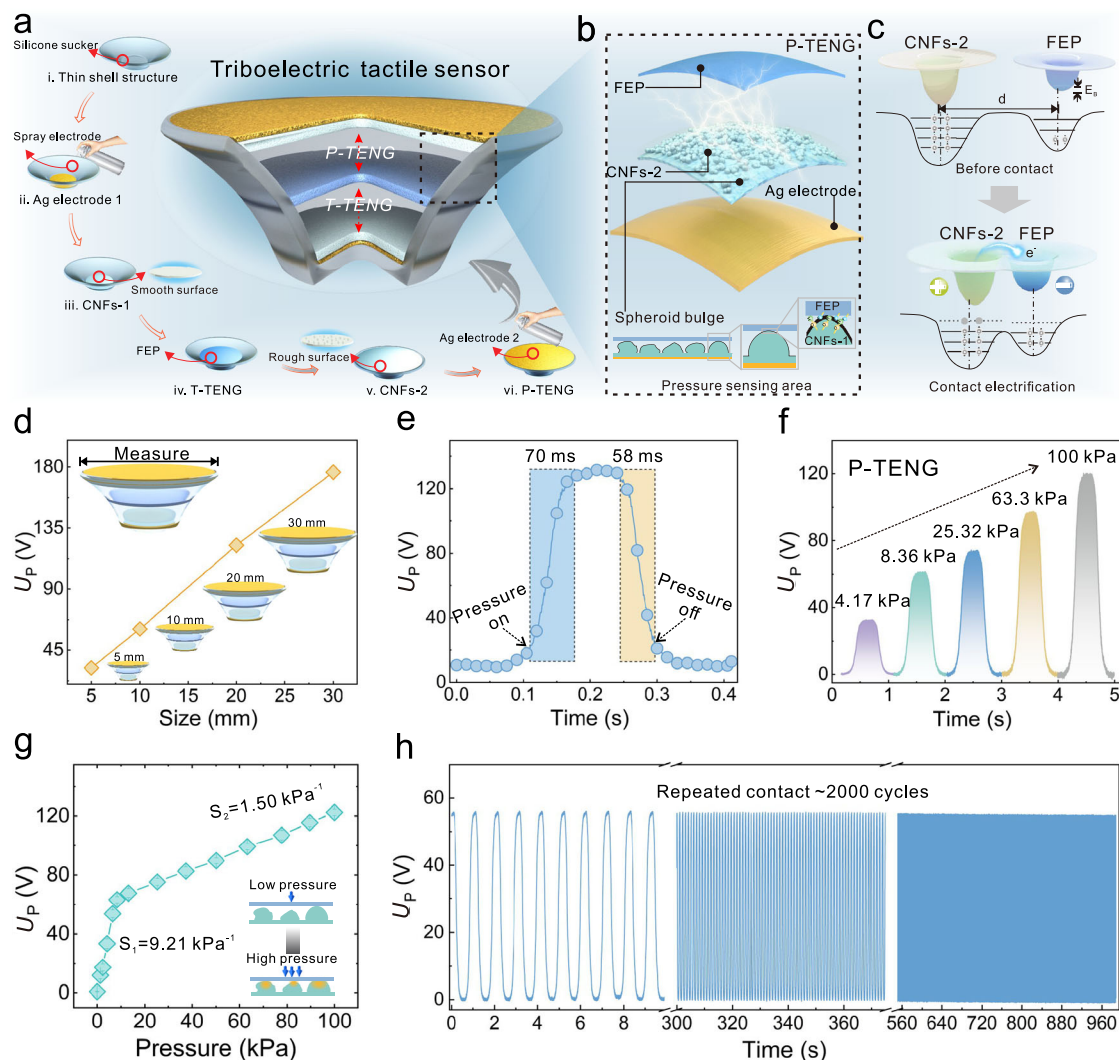
Fig. 3 | Pressure sensing. a Schematic diagram of the preparation process of the triboelectric sensor, FEP is fluorinated ethylene propylene, CNFs are cellulose nanofibrils. **b** Structure of pressure sensor (P-TENG). **c** The response mechanism of pressure sensing. **d** Scalable preparation of the triboelectric sensor, U_P is the voltage generated by the pressure sensor. **e** Response time of P-TENG. **f** Triboelectric signals of P-TENG. **g** Pressure sensing sensitivity of P-TENG. Data were presented as mean values ± SD. **h** Stability test of P-TENG.

8.36–100 kPa, the sensitivity of the triboelectric signal is 1.5 kPa^{-1} (Eq. 1).

$$S = d(\Delta V / V_s)/dP \qquad (1)$$

Where ΔV is the relative change of the output voltage, V_s is the minimum detectable electrical signal, and P is the applied pressure. In the high-pressure range, the open-circuit voltage gradually increases, which is due to the increase of the area when the surface microstructure of the material is contacted, thus enhancing the triboelectric effect[36,39,42]. It is also highlighted that the sensitivity of the P-TENG is one of the highest levels among the current triboelectric tactile sensors (Supplementary Table 2). To further verify the applicability in extreme environments, after 2000 cycles of testing at 200 °C, the output performance of the sensor did not change significantly (Fig. 3h), demonstrating the durability and high-temperature robustness of the P-TENG.

Temperature-responsive behaviors

Temperature affects the magnitude of the triboelectric signals[30,35,43,44], hence, the T-TENG was developed to respond to temperature stimuli. The

Figure 4a illustrates the structure and working mechanism of T-TENG. Under the heat stimulus, the temperature of the triboelectric materials increases, leading to the disordered dissipation of stored charges[45]. This phenomenon is further explained by the electron-cloud model under high temperatures (Fig. 4b). When the two materials contact, the electron cloud overlaps, the initial single potential well becomes an asymmetric double potential well, and the electrons transfer to generate the triboelectric signal. In this context, the improved thermionic emission model (Supplementary Note 3) indicates that the output voltage of T-TENG decreases with rising temperature[46], which facilitates temperature sensing due to the emission of triboelectric charges caused by the increase in temperature.

Figure 4c shows the continuous voltage response to temperature, exhibiting distinguishable and stable signals. At 2 Hz, the response times are 67 and 63 ms, respectively, which are close to those of the P-TENG (Supplementary Fig. 11). The linear response coefficient of sensitivity for the T-TENG is 0.996, indicating a good linear relationship between the electrical signal and temperature. Notably, the T-TENG exhibits pressure insensitivity in temperature sensing (Fig. 4d). This may be attributed to the smooth surface and constant contact area, making the pressure value quickly reach equilibrium[47]. The
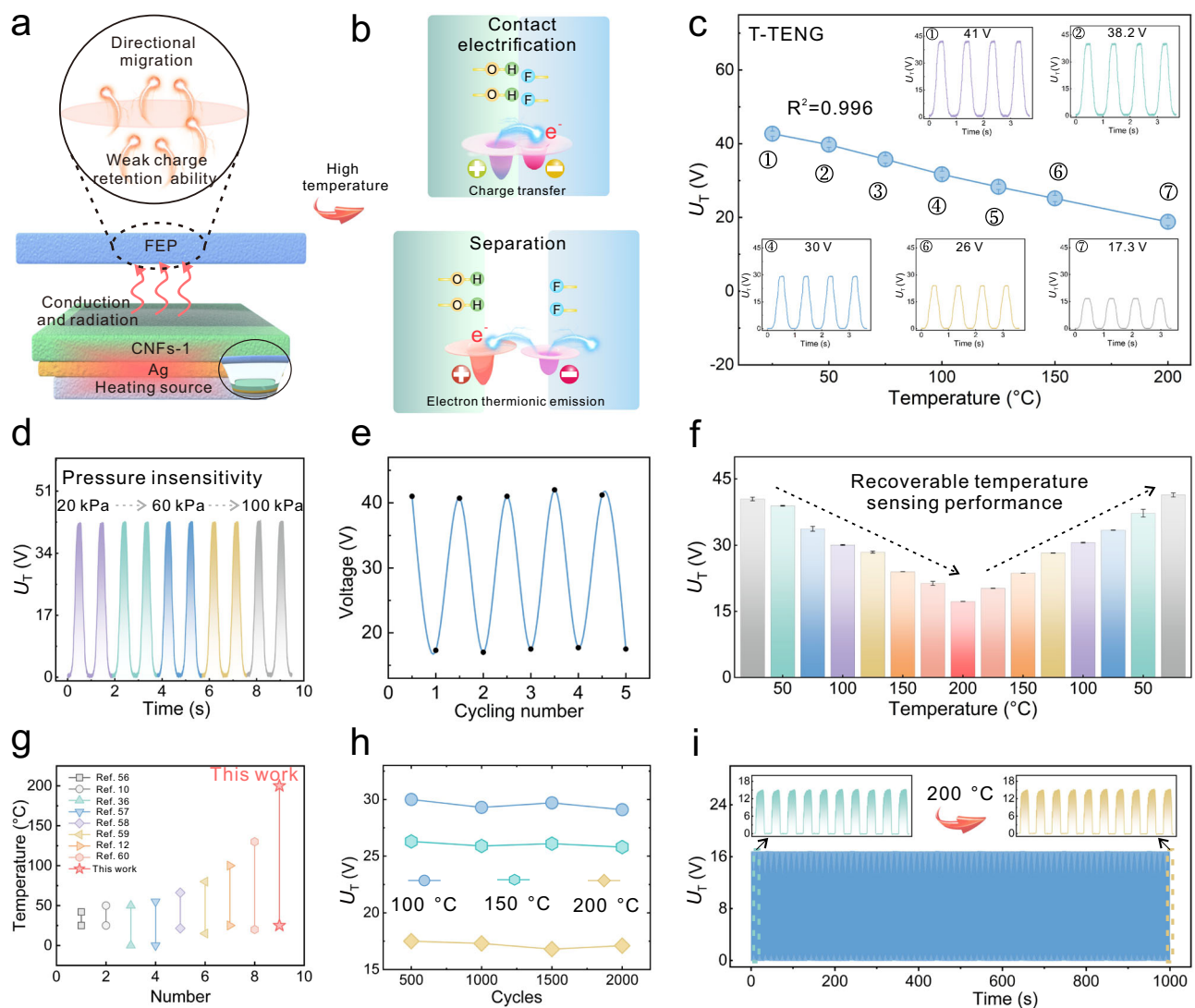
Fig. 4 | Temperature sensing. a, b Schematic diagram of the mechanism of temperature sensor (T-TENG). **c** Temperature sensing data. Data were presented as mean values ± SD, U_T is the voltage generated by the temperature sensor. **d** Pressure-insensitivity of T-TENG. **e** Temperature cycle test of T-TENG at 25 °C and 200 °C. **f** Recoverable sensing capability of T-TENG. Data were presented as mean values ± SD. **g** Comparison of T-TENG with other literature[10,12,36,56–60]. **h, i** Stability test of T-TENG at high temperatures.

sensor signals show high consistency with temperature changes, and highly repeatable output voltages are observed during the heating-cooling cycles (Fig. 4e, f), demonstrating the real-time adaptability of the sensing signal to the ambient temperature. About 2000 cycles of testing were performed at 100, 150, and 200 °C, respectively (Fig. 4h), and the open-circuit voltage of the T-TENG during the loading-unloading process at 200 °C was taken as an example (Fig. 4i). The results show stable sensing signals, proving the T-TENG's suitability for practical sensing in high-temperature environments. The T-TENG sensor has a wide range and beyond human skin temperature sensing ability (25–200 °C), superior to the self-powered temperature sensors reported in the literatures (Fig. 4g), offering opportunities for the development of temperature perception and human-machine interaction in extreme environments.

Mechanism study for the multimodal response

In practical applications, multiple stimuli need to be detected simultaneously and independently. The signal interference between multiple coupled stimuli will affect the accuracy of the sensor, which requires the sensor to have low cross-interference and stable decoupling ability for the coupled signals (Fig. 5a). The signal interference of

multimodal triboelectric sensors under fixed pressure and different temperatures was discussed (Fig. 5b). Compared with theoretical results (Supplementary Fig. 12), the cross-coupling errors of P-TENG and T-TENG due to temperature interference are less than 0.4 and 3.2%, respectively, indicating low cross-sensitivity between pressure and temperature. The low cross-sensitivity stems from the independence between the response mechanisms of pressure and temperature stimulus (thermionic emission effect and contact area effect). The pressure response of P-TENG under different temperatures was further tested (Fig. 5c), and there was still a linear response between the pressure and voltage of the P-TENG (U_P) at different temperatures. The relationship between U_P and voltage of the T-TENG (U_T) and pressure and temperature can be related by the characteristic matrix (M) (Supplementary Note 4).

The feature matrix constructed from the linear dependence of the multimodal triboelectric sensor can be directly used for the stable decoupling of multiple signals. With known subcomponents of the feature matrix, unknown pressure (P) and temperature (T) can be obtained using the M and the values of U_P and U_T. Figure 5d shows the corresponding relationship between pressure, temperature, and U_P. Through feature matrix analysis, it's evident that components M_3 and
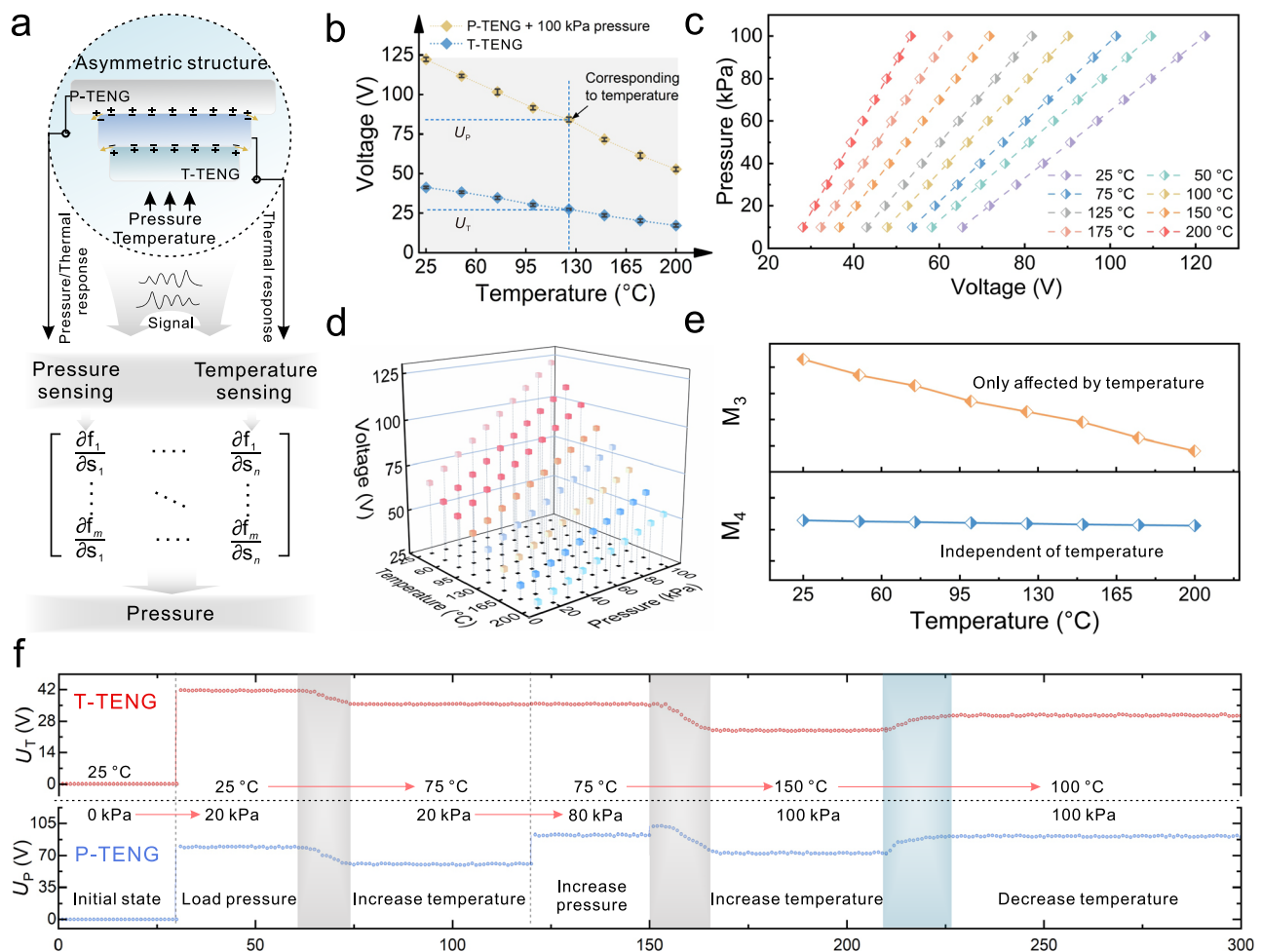
Fig. 5 | Pressure-temperature decoupling and dual-modal sensing in a single triboelectric sensor. a Simultaneous extraction of two sensing parameters (pressure and temperature) by the matrix method. **b** Response signals of P-TENG and T-TENG at different temperatures under the pressure of 100 kPa. Data were presented as mean values ± SD. **c** Pressure parameters corresponding to the voltage signals of P-TENG at different temperatures. **d** Voltage signals of P-TENG when both pressure and temperature are applied. **e** Variation of the M_3 and M_4 of the matrix under different temperatures. **f** Real-time response of the triboelectric sensor when subjected to temperature and pressure stimuli.

M_4 are directly related to P-TENG, and M_3 has a mutual dependence on temperature (Fig. 5e). Figure 5f and Supplementary Fig. 13 demonstrate the real-time response of the triboelectric sensor in complex scenarios with multiple coupled stimuli. Stable electrical signal responses can be achieved under conditions of individually varying temperature and pressure, as well as simultaneously varying pressure and temperature. Furthermore, to verify the sensor's potential in real complex scenarios, the stability of the signals in high humidity and strong ultraviolet irradiation environments was studied (Supplementary Fig. 14). It can be observed that the sensor's electrical signals are stable, benefiting from the stability of the material and the encapsulation of the shell and electrodes. The demonstrations above verify the sensors' low cross-sensitivity to temperature and pressure signals, enabling the decoupling of dual stimuli through the feature matrix, and contributing to high-precision measurements in practical complex applications.

Real-time object recognition in high-temperature environments

Robotics technology utilizes multimodal sensors and combines artificial intelligence technology, unlocking intelligent data analytics in interdisciplinary, and achieving complex gesture and object recognition[48,49]. Therefore, to better demonstrate the pressure/temperature-responsive capabilities of the tactile sensor in practical scenarios, the sensors are integrated into the five fingertips of a robotic

hand, forming an intelligent tactile system for identifying unknown objects (Fig. 6a). Stretchable electrodes were designed to ensure the flexibility of hand movements (Fig. 6a inset), avoiding the interference of electrode damage to the signal. The system can remotely control the robot hand and simulate various hand movements synchronously, providing users with spatially distributed tactile feedback (Fig. 6b and Supplementary Movie 2), and offering a direction for replacing humans in potentially hazardous tasks in complex extreme environments.

Further, various contact commands are issued in the high-temperature environment for the identification of object shape and temperature. A multichannel data acquisition module is used to simultaneously receive and analyze the triboelectric signals collected from the five fingers during the grasping process. The triboelectric sensors on the inner side of the robot hand obtain different signals when grasping objects of different temperatures and shapes (spherical iron balls, square wooden blocks, and hollow cylinders). The triboelectric signals are normalized to obtain the electric signal maps corresponding to the grasped objects (Supplementary Movie 3). The signal maps from top to bottom represent the output signals of T-TENG and P-TENG, respectively, where darker colors indicate higher signal outputs (Fig. 6c). For instance, grasping spherical and square objects of different sizes and shapes at room temperature results in different output signals due to gripping habits, varied number of
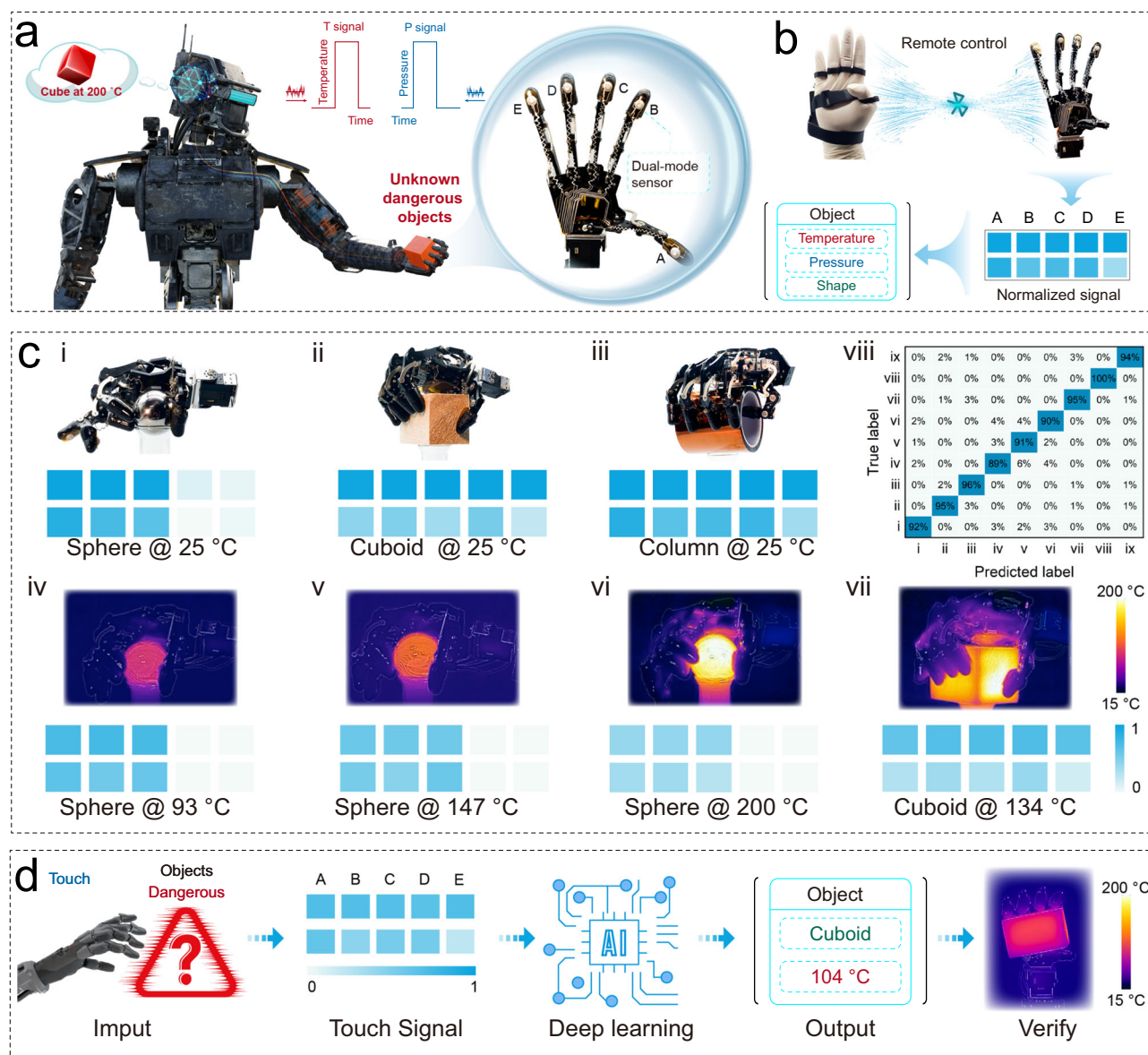
Fig. 6 | Tactile perception in high-temperature environments. a Schematic diagram of tactile perception, the inset shows the optical image of the sensor integrated into the robot hand. **b** Schematic diagram of the robot hand for remote control and identification of objects (A, B, C, D, and E stand for thumb, index finger, middle finger, ring finger, and little finger, respectively). **c** Robot hand with integrated triboelectric sensors for object shape and temperature recognition in complex environments. **d** Intelligent tactile sensing system based on triboelectric signals and deep learning.

fingertips, and differing force exertion (Fig. 6ci–iii). Meanwhile, when changing the temperature and shape, the number and intensity of electrical signals also vary (Fig. 6civ–vii).

Combining neural network learning with tactile sensors for perception is an effective approach to object recognition issues in the context of robot technology. Machine learning based on convolutional neural networks can extract subtle differences and complex features from signals. Through numerical optimization methods, neural networks can actively discover features hidden in signals during the training process, thereby establishing decision criteria. Fig. 6cviii shows the confusion matrix of the classification results of 9 objects, where each row represents a test sample in an actual category, and each column represents a predicted category. The results demonstrate that the system has excellent recognition performance for symmetric and asymmetric objects (Supplementary Fig. 15), with an average recognition accuracy of 94%. Furthermore, as a conceptual validation, the sensing system was used to identify the types and temperatures of objects (Fig. 6d). The robot tactile perception system enables object

identification in high-temperature environments, possessing potential applications in fields beyond human touch perception such as human-machine interaction in extreme environments and space exploration.

Discussion

In summary, this work demonstrates a triboelectric tactile sensor that responds to pressure/temperature beyond the human tactile perception range in extreme environments. The tactile sensor is based on the triboelectric nanogenerator technology, using stable cellulosic triboelectric materials under high temperature, and designed an asymmetric structure that can independently output dual signals, to achieve multiple stimulation responses in high-temperature environments. The device achieves real-time digital response without an external power supply, and the feature of size-switchable is conducive to scalable integration. Combining machine learning technology can further accurately identify the shape and temperature of objects in high-temperature environments. The proposed self-powered multimodal sensing system provides a design idea for the development of cutting-

edge human-machine interaction. However, this work is still in the preliminary research stage, and can further achieve complex applications in extreme environments through multidisciplinary integration (such as the design of heat-insulating and flame-retardant materials and the expansion of wireless plugins, etc.).

Methods

Materials
3-Aminopropyltriethoxysilane (APTES) was obtained from Aladdin, and all purchased chemicals were of analytical purity. Bagasse pulpboard was obtained from Guangxi Guitang (China) Co., Ltd. The FEP, silver paint, silicone shell, and high-temperature adhesive were purchased from Tmall.

Preparation of triboelectric materials
High-purity cellulose material was obtained by purifying bagasse pulpboard and then transformed into nanoscale size by high-pressure homogenization[50,51]. With a slurry concentration of 1%, the dry weight of the sample was determined to be 0.4 g. The CNFs film material (thickness $63 \pm 4 \, \mu m$) was prepared by vacuum-assisted fibril self-assembly followed by hot pressing and drying[52,53]. Then, the CNFs film was treated by low-temperature plasma technology, with oxygen as the discharge gas, at a power of 100 W for 10 min, to obtain a CNFs film with micro-nano structures on the surface[54]. Subsequently, the CNFs film and a CNFs film with protruding structures were separately immersed in a 3 wt% APTES solution for 2 h, then sufficiently washed with ethanol and dried in an oven at 120 °C to obtain the final temperature sensing material CNFs-1 film and pressure sensing material CNFs-2 film. The detailed preparation process is shown in Supplementary Fig. 4a.

Preparation of triboelectric sensor
The CNFs-1 film with a diameter of 5 mm and coated with Ag on the back is adhered to the silicone shell (bottom diameter 10 mm, top diameter 5 mm) as the positive triboelectric material of the T-TENG. Subsequently, the FEP (diameter 7.5 mm), serving as the common negative triboelectric material for the multimodal sensor, is attached to the middle of the silicone shell. Finally, the circular CNFs-2 film with a diameter of 10 mm is attached to the bottom of the shell, and conductive copper wires are respectively attached to the backs of the CNFs-1 and CNFs-2 films, thus forming a single-electrode mode multimodal sensor. Lastly, the silver paint is sprayed onto the surface of the sensor.

Performance testing of triboelectric sensor
The electrical performance of the dual TENGs was measured using an electrometer (Keithley 6514, USA). For standard measurement of electrical output, a commercial linear mechanical motor is used to apply a constant contact force, with the magnitude of the applied force measured by a HYPX-601 instrument. The prepared T-TENG and P-TENG are respectively attached to the fixed side of the motor, and pressure is applied to the devices using a linear motor. The generated electrical signals are measured by the electrometer, then collected by a data acquisition card (NI-USB6259, USA), and the final data were transferred to computer software for display. A multichannel switch multimeter (Keithley DAQ6510, USA) was used to record multiple signals of the multimodal tactile sensor. A schematic diagram of the experimental setup is shown in Supplementary Fig. 16.

Selection of the installation positions on the robot hand for the triboelectric tactile sensors
To identify objects more accurately with a small number of sensors, the sensor position needs to be optimized. Therefore, before installing the sensors on the robotic hand, the hand was used to grasp colored objects, and then the colored positions were recorded and counted. It was found that the fingertips were used the most during the gripping process[7,55].

Characterizations
The surface morphology of the material was analyzed by a scanning electron microscope (TESCAN MIRA LMS) and an atomic force microscope (BRUKER, USA). A Fourier transform infrared spectrometer (TENSOR II, BRUKER, Germany) was used to observe the chemical changes of the samples, and a simultaneous thermal analyzer (TG 209 F3 Tarsus, Germany) was used to test the thermodynamic behavior of the materials. The COMSOL Multiphysics software was used to study the electric potential distribution of the triboelectric materials during contact electrification, with the thicknesses of FEP and CNFs-2 set at 50 and 63 μm, respectively. Density functional theory (DFT) calculations were performed using the Vienna ab initio Simulation Package (VASP) combined with the projector augmented wave method. The Perdew-Burke-Ernzerhof (PBE) functional, following the generalized gradient approximation, was employed for the exchange-correlation functional. A $2 \times 2 \times 1$ K-point grid was used for sampling the Brillouin zone, and the energy cutoff was fixed at 500 eV. Structural relaxation continued until the convergence thresholds for energy and force were met at 1×10^{-4} eV and 0.03 eV Å^{-1}, respectively.

Data availability
All data generated in this study are provided in the Supplementary Information/Source Data file. Source data are provided with this paper.

References

1. Kaur, M., Kim, T. H. & Kim, W. S. New frontiers in 3D structural sensing robots. *Adv. Mater.* **33**, 2002534 (2021).
2. Zhang, J. et al. Finger-inspired rigid-soft hybrid tactile sensor with superior sensitivity at high frequency. *Nat. Commun.* **13**, 5076 (2022).
3. Li, G. et al. Self-powered soft robot in the Mariana Trench. *Nature* **591**, 66–71 (2021).
4. Lu, H. et al. A bioinspired multilegged soft millirobot that functions in both dry and wet conditions. *Nat. Commun.* **9**, 3944 (2018).
5. Li, S. et al. Bioinspired robot skin with mechanically gated electron channels for sliding tactile perception. *Sci. Adv.* **8**, eade0720 (2022).
6. Lee, S. et al. Beyond human touch perception: an adaptive robotic skin based on gallium microgranules for pressure sensory augmentation. *Adv. Mater.* **34**, 2204805 (2022).
7. Zhang, Y. et al. Localizing strain via micro-cage structure for stretchable pressure sensor arrays with ultralow spatial crosstalk. *Nat. Commun.* **14**, 1252 (2023).
8. Huang, Y. et al. A skin-integrated multimodal haptic interface for immersive tactile feedback. *Nat. Electron.* **6**, 1020–1031 (2023).
9. Wang, X.-Q. et al. In-built thermo-mechanical cooperative feedback mechanism for self-propelled multimodal locomotion and electricity generation. *Nat. Commun.* **9**, 1–10 (2018).
10. Lee, J. H. et al. Rational design of all resistive multifunctional sensors with stimulus discriminability. *Adv. Funct. Mater.* **32**, 2107570 (2022).
11. An, B. W., Heo, S., Ji, S., Bien, F. & Park, J.-U. Transparent and flexible fingerprint sensor array with multiplexed detection of tactile pressure and skin temperature. *Nat. Commun.* **9**, 2458 (2018).
12. Wang, P., Yu, W., Li, G., Meng, C. & Guo, S. Printable, flexible, breathable and sweatproof bifunctional sensors based on an all-nanofiber platform for fully decoupled pressure–temperature sensing application. *Chem. Eng. J.* **452**, 139174 (2023).
13. Sun, Z., Zhu, M., Shan, X. & Lee, C. Augmented tactile-perception and haptic-feedback rings as human-machine interfaces aiming for immersive interactions. *Nat. Commun.* **13**, 5224 (2022).

14. Qiu, X., Liu, J., Zhou, B. & Zhang, X. Bioinspired bimodal mechanosensors with real-time, visualized information display for intelligent control. *Adv. Funct. Mater.* **33**, 2300321 (2023).

15. Yang, W. et al. Self-powered interactive fiber electronics with visual–digital synergies. *Adv. Mater.* **33**, 2104681 (2021).

16. Tien, N. T. et al. A flexible bimodal sensor array for simultaneous sensing of pressure and temperature. *Adv. Mater.* **26**, 796–804 (2014).

17. Liu, L. et al. Progress of triboelectric nanogenerators with environmental adaptivity. *Adv. Funct. Mater.* **34**, 2308353 (2023).

18. Lee, M. M. The robot explorers. *Sci. Robot.* **6**, eabj8903 (2021).

19. Fu, M. et al. A highly sensitive, reliable, and high-temperature-resistant flexible pressure sensor based on ceramic nanofibers. *Adv. Sci.* **7**, 2000258 (2020).

20. Wang, S. et al. Flexible optoelectronic multimodal proximity/pressure/temperature sensors with low signal interference. *Adv. Mater.* **35**, 2304701 (2023).

21. Gao, F.-L. et al. Ti3C2T x MXene-based multifunctional tactile sensors for precisely detecting and distinguishing temperature and pressure stimuli. *ACS Nano* **17**, 16036–16047 (2023).

22. Tao, X. et al. Triboelectric polymer with high thermal charge stability for harvesting energy from 200 C flowing air. *Adv. Funct. Mater.* **31**, 2106082 (2021).

23. Wei, X., Wang, B., Wu, Z. & Wang, Z. L. An open-environment tactile sensing system: toward simple and efficient material identification. *Adv. Mater.* **34**, 2203073 (2022).

24. Shao, Y. et al. Harvesting energy from extreme environmental conditions with cellulosic triboelectric materials. *Mater. Today* **66**, 348–370 (2023).

25. Gao, C. et al. Cellulosic triboelectric materials for stable energy harvesting from hot and humid conditions. *Nano Energy* **111**, 108426 (2023).

26. Xu, P. et al. A bio-inspired and self-powered triboelectric tactile sensor for underwater vehicle perception. *npj Flex. Electron.* **6**, 25 (2022).

27. Liu, Y. et al. Enhancement of triboelectric charge density by chemical functionalization. *Adv. Funct. Mater.* **30**, 2004714 (2020).

28. Zhang, S. et al. Bioinspired asymmetric amphiphilic surface for triboelectric enhanced efficient water harvesting. *Nat. Commun.* **13**, 4168 (2022).

29. Wang, H. et al. A paradigm shift fully self-powered long-distance wireless sensing solution enabled by discharge-induced displacement current. *Sci. Adv.* **7**, eabi6751 (2021).

30. Lin, S., Xu, C., Xu, L. & Wang, Z. L. The overlapped electron-cloud model for electron transfer in contact electrification. *Adv. Funct. Mater.* **30**, 1909724 (2020).

31. Cheng, B. et al. High performance temperature difference triboelectric nanogenerator. *Nat. Commun.* **12**, 4782 (2021).

32. Chi, M. et al. Tunable anisotropic structural aramid triboelectric aerogels enabled by magnetic manipulation. *Adv. Funct. Mater.* **34**, 2310280 (2023).

33. Shi, N. N. et al. Keeping cool: enhanced optical reflection and radiative heat dissipation in Saharan silver ants. *Science* **349**, 298–301 (2015).

34. Syeda, R. et al. Piezo1 channels are inherently mechanosensitive. *Cell Rep.* **17**, 1739–1746 (2016).

35. Lin, S. et al. Electron transfer in nanoscale contact electrification: effect of temperature in the metal–dielectric case. *Adv. Mater.* **31**, 1808197 (2019).

36. Zhang, H. et al. Bioinspired chromotropic ionic skin with in-plane strain/temperature/pressure multimodal sensing and ultrahigh stimuli discriminability. *Adv. Funct. Mater.* **32**, 2208362 (2022).

37. Zhu, L. et al. Highly temperature resistant cellulose nanofiber/polyvinyl alcohol hydrogel using aldehyde cellulose nanofiber as cross-linker. *Cellulose* **26**, 5291–5303 (2019).

38. Lu, D. et al. Wearable triboelectric visual sensors for tactile perception. *Adv. Mater.* **35**, 2209117 (2023).

39. Liu, T. et al. Nanocellulosic triboelectric materials with micromountain arrays for moisture-resisting wearable sensors. *Nano Energy* **112**, 108480 (2023).

40. Lakshminarayanan, K. et al. The effect of tactile imagery training on reaction time in healthy participants. *Brain Sci.* **13**, 321 (2023).

41. Kasozi, K. I. et al. A study on visual, audio and tactile reaction time among medical students at Kampala International University in Uganda. *Afr. Health Sci.* **18**, 828–836 (2018).

42. Zhang, W. et al. Spheres multiple physical network-based triboelectric materials for self-powered contactless sensing. *Small* **18**, 2200577 (2022).

43. Shen, S. et al. Triboelectric polymer with excellent enhanced electrical output performance over a wide temperature range. *Nano Energy* **110**, 108347 (2023).

44. Shi, F., Wei, X., Wang, H. & Wu, X. Electrospun polyimide nanofiber-based triboelectric nanogenerator for harvesting energy at elevated temperatures. *ACS Appl. Electron. Mater.* **4**, 4569–4575 (2022).

45. Lu, C. X. et al. Temperature effect on performance of triboelectric nanogenerator. *Adv. Eng. Mater.* **19**, 1700275 (2017).

46. Xu, C. et al. Raising the working temperature of a triboelectric nanogenerator by quenching down electron thermionic emission in contact-electrification. *Adv. Mater.* **30**, 1803968 (2018).

47. Bae, G. Y. et al. Pressure/temperature sensing bimodal electronic skin with stimulus discriminability and linear sensitivity. *Adv. Mater.* **30**, 1803388 (2018).

48. Kwon, S. Y. et al. On-skin and tele-haptic application of mechanically decoupled taxel array on dynamically moving and soft surfaces. *npj Flex. Electron.* **6**, 98 (2022).

49. Wen, F., Zhang, Z., He, T. & Lee, C. AI enabled sign language recognition and VR space bidirectional communication using triboelectric smart glove. *Nat. Commun.* **12**, 5378 (2021).

50. Zhang, C. et al. Chemically functionalized cellulose nanofibrils-based gear-like triboelectric nanogenerator for energy harvesting and sensing. *Nano Energy* **66**, 104126 (2019).

51. Nie, S. et al. Enzymatic and cold alkaline pretreatments of sugarcane bagasse pulp to produce cellulose nanofibrils using a mechanical method. *Ind. Crop. Prod.* **124**, 435-441 (2018).

52. Liu, Y. et al. Chemically tailored molecular surface modification of cellulose nanofibrils for manipulating the charge density of triboelectric nanogenerators. *Nano Energy* **89**, 106369 (2021).

53. Wang, J. et al. Dynamic thermostable cellulosic triboelectric materials from multilevel-non-covalent interactions. *Small* **20**, 2307504 (2023).

54. Huang, C. et al. Surface characterization of plasma-treated eucalyptus alkaline peroxide mechanical pulp using electronic spectroscopy chemical analysis and atomic force microscopy. *BioResources* **13**, 3500–3510 (2018).

55. Li, G., Liu, S., Wang, L. & Zhu, R. Skin-inspired quadruple tactile sensors integrated on a robot hand enable object recognition. *Sci. Robot.* **5**, eabc8134 (2020).

56. Choi, W. Y., Kwon, J. H., Kim, Y. M. & Moon, H. C. J. S. Multimodal wearable ionoskins enabling independent recognition of external stimuli without crosstalk. *Small* **19**, 2301868 (2023).

57. Xiao, H. et al. Dual mode strain–temperature sensor with high stimuli discriminability and resolution for smart wearables. *Adv. Func. Mater.* **33**, 2214907 (2023).

58. Zhao, H. et al. Intelligent recognition using ultralight multifunctional nano-layered carbon aerogel sensors with human-like tactile perception. *Nanomicro Lett.* **16**, 11 (2024).

59. Fan, L., Yang, X. & Sun, H. J. A novel flexible sensor for double-parameter decoupling measurement of temperature and pressure

with high sensitivity and wide range. *J. Mater Chem*. **11**, 10163-10177 (2023).

60. Zhang, F., Zang, Y., Huang, D., Di, C.-A. & Zhu, D. Flexible and self-powered temperature–pressure dual-parameter sensors using microstructure-frame-supported organic thermoelectric materials. *Nat. Commun*. **6**, 8356 (2015).

Acknowledgements

Author contributions

The overall experimental design was conceived by Y.L. and S.N., and together, they coordinated the full project. Y.L., J.W., and T.L. constructed the system hardware and software platform, proposed the theory, and performed the experiments. Z.W. and B.L. fabricated TENG and carried out data collection and analysis. M.C., S.Z., C.C., C.G., and T.Z. characterized and analyzed the materials. All authors also discussed and interpreted the experimental data and results. Y.L. and J.W. wrote the manuscript with contributions from all authors. S.W. and S.N. reviewed and edited the paper.

Competing interests

The authors declare no competing interests.

Additional information

Supplementary information The online version contains supplementary material available at https://doi.org/10.1038/s41467-024-55771-0.

Correspondence and requests for materials should be addressed to Shuangxi Nie.

Reprints and permissions information is available at http://www.nature.com/reprints

Publisher's note Springer Nature remains neutral with regard to jurisdictional claims in published maps and institutional affiliations.